

Supporting Information for:

Systematic electrochemical oxidative doping of P3HT to probe interfacial charge transfer across polymer-fullerene interfaces

*Judith L. Jenkins,^{a,b} Paul A. Lee,^a Kenneth W. Nebesny^a Erin L. Ratcliff^{*c}*

* Corresponding author: ratcliff@email.arizona.edu

^a Department of Chemistry and Biochemistry, University of Arizona, 85721

^b Present address: Department of Chemistry, Eastern Kentucky University, 40475

^c Department of Materials Science, University of Arizona, 85721

Table of Contents:

SI1: e-P3HT/C₆₀ solar cell data

SI2: Additional P3HT optical spectra

SI3: Additional e-P3HT/C₆₀ XPS spectra and discussion of peak fitting

SI4: Additional e-P3HT/C₆₀ UPS spectra

SI1: e-P3HT/C₆₀ solar cell data

Organic thin-films were deposited via vacuum deposition (1 Å/s) at base pressures of 10^{-7} Torr via Knudsen-type sublimation cells, monitored with a 10 MHz quartz crystal microbalance (QCM-Newark), and an Agilent Technologies frequency monitor (Model 53131A). Aluminum top contacts were deposited at pressures no greater than 10^{-6} Torr at a deposition rate of 1–3 Å/s, monitored via a 6 MHz QCM (Tangidyne) and Inficon deposition monitor (Model 758-500-G1). These aluminum top contacts defined the device area of 0.0716 cm². Current–voltage (J/V) data was obtained for several solar cells for each polymer film with different oxidation potentials. The J/V data presented here are representative of at least five devices. Solar cell testing was carried out in a N₂-filled double-glovebox (MBrawn Labmaster), with water and oxygen levels at less than 0.1 ppm. Current–voltage measurements were made with a Keithley 2400 source meter, while the data was acquired with in-house software created with *Labview* ver.8.2 (National Instruments). Scans ranged from –1.00 to 1.50 V using a 20 mV step starting from negative bias. A CUDA products light source with a 250 W quartz-halogen lamp (Model I-250) was used as the illumination source. The light was filtered with a 750 nm cutoff filter, along with a sand-blasted light diffuser. The distance to the device arrays was adjusted to achieve an output of approximately 100 mW/cm², as measured with an Apogee PYR-S pyranometer.

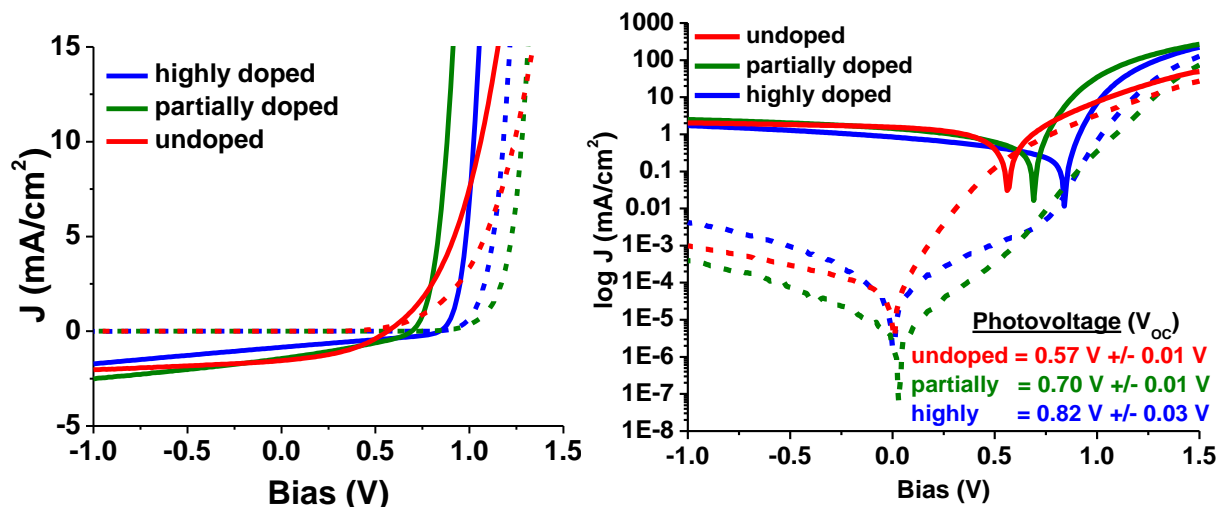


Figure S11: Current density-voltage curves generated from solar cells built using the e-P3HT/C₆₀ heterojunctions are shown as a function of polymer oxidative doping. The full device configuration is ITO/e-P3HT/C₆₀/BCP/Al, and the solar cells were tested in both the dark (dotted lines) and the light (100 mW simulated AM 1.5G; solid lines). Data from five large-area devices (electrode area = 0.0716 cm²) were averaged to yield these V_{OC} values. The trends for V_{OC} and J_{SC} predicted by the frontier energy levels of the active layer components were observed in these devices. The largest J_{SC} was measured for the undoped e-P3HT/C₆₀ interface, while the largest V_{OC} was measured for the highly doped e-P3HT/C₆₀ interface.

Because of the charge redistribution detected at these e-P3HT/C₆₀ interfaces, and the suggested correlations between the D/A interface ΔE_{DA} and V_{OC},¹ the differences between predicted ΔE_{DA} and measured V_{OC} values were examined in more detail. There are many synergistic explanations of the differences in device performance observed here, but we choose to look briefly at V_{OC}. Note that when interfacial charge redistribution was detected (undoped and partially doped e-P3HT), the measured V_{OC} is closer to that approximated by ΔE_{DA} . When no interfacial charge redistribution occurred (highly doped e-P3HT) V_{OC} is 0.5 V below its theoretical maximum value, representative of a significant loss of device power. While a full explanation of this device behavior is beyond the scope of this work, these results do affirm the need for strategic control of local interfacial chemistry in achieving the desired device functionality, in addition to synthetic control of individual materials optoelectronic properties.

Table S11: Solar cell data from e-P3HT/C₆₀ active layers as a function of oxidative doping; data from five large-area devices (electrode area = 0.0716 cm²) were averaged to yield these values

	Highly doped (+ 1.0 V)	Partially doped (+ 0.6 V)	Undoped (0.0 V)
J₀ (mA/cm²)	-1.39 (±1.07)*10 ⁻⁶	-5.42 (±8.10)*10 ⁻⁷	-4.76 (±1.86)*10 ⁻⁶
J_{sc} (mA/cm²)	-0.75 (±0.10)	-1.23 (±0.17)	-1.51 (±0.10)
V_{oc} (V)	0.82 (±0.03)	0.70 (±0.01)	0.57 (±0.01)
Fill Factor	0.2988 (±0.0248)	0.3023 (±0.0170)	0.3875 (±0.0076)

SI2: Additional P3HT optical spectra

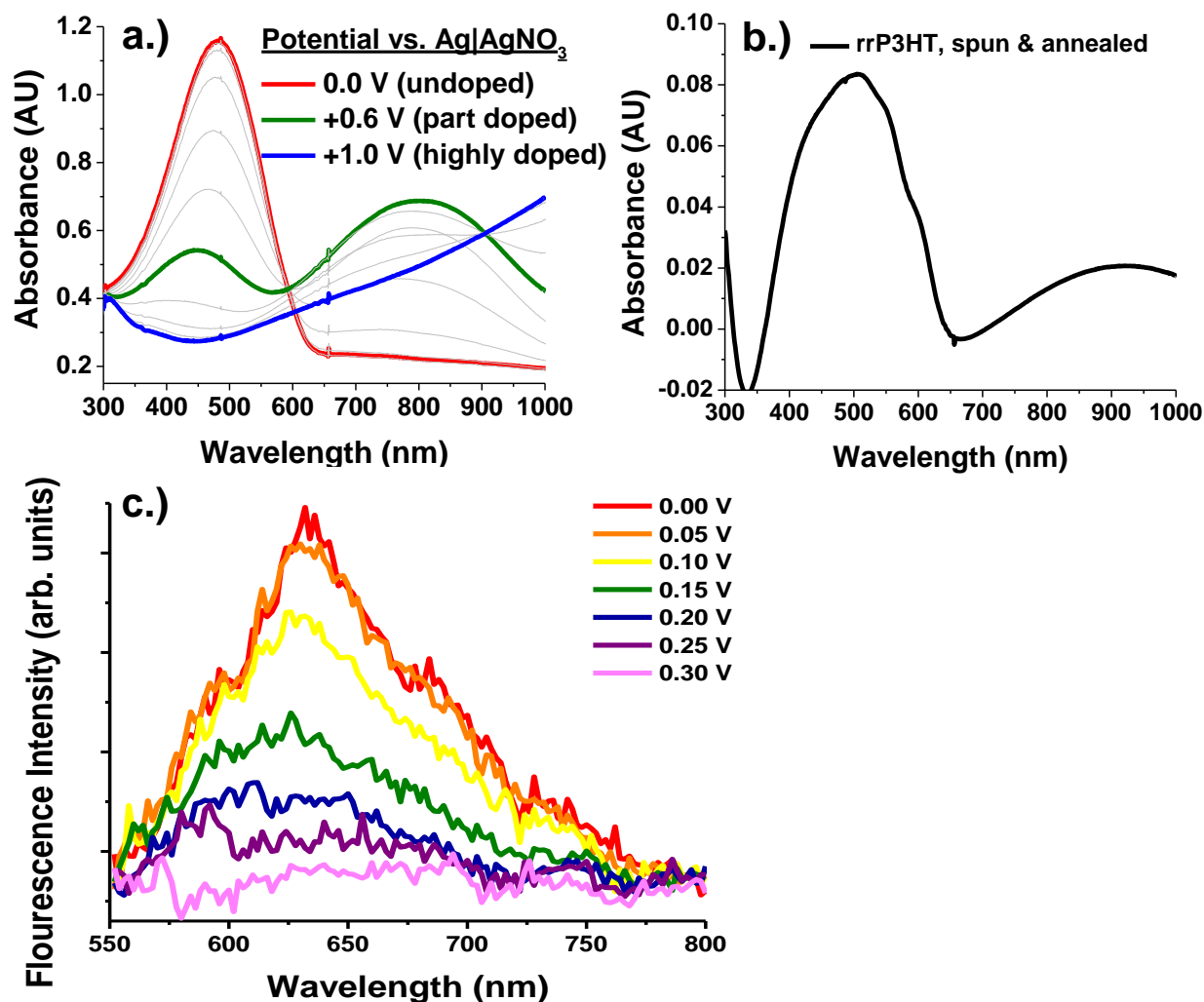


Figure SI2: Potential-dependent absorbance spectra of e-P3HT (a) and potential-dependent fluorescence spectra (c) of e-P3HT² on ITO illustrate the differences in polaronic density achieved through electrochemical oxidative doping. All potentials are reference to Ag|AgNO₃ (10 mM). A spectrum of spuncast and annealed regioregular P3HT (rrP3HT) is shown for reference (b).

SI3: Additional XPS spectra of the e-P3HT/C₆₀ heterojunction and discussion of peak fitting

Figure SI3.1 illustrates the C 1s spectral features associated with the four different carbon species in a fully-oxidized e-P3HT film including the alkyl carbons, the neutral aromatic carbons, the polaronic carbons, and the bipolaronic carbons.² The deposition of C₆₀ led to increases in the neutral aromatic peak.³ The spectral subtraction used to effectively analyze the S 2p spectra is not possible with the C 1s spectra, due to the additional carbon signal from the C₆₀. Instead, to quantify changes in the degree of polymer oxidation during interface formation, it was necessary to fit each spectrum with five Gaussian peaks corresponding to each of different carbon species. The alkyl carbon peak was fit first, and the intensity of this peak (corresponding to 60 % of signal from e-P3HT) was used to determine the total C 1s intensity due to e-P3HT. The remaining C 1s spectral intensity was attributed to C₆₀. Once the alkyl feature was fit, the polaronic and bipolaronic contributions were fit. Finally, the remaining polymer intensity was assigned to neutral aromatic carbons in e-P3HT.

Though harder to quantify, the C 1s spectra in Figure SI3.2 show ~10 % increases in the spectral intensity coming from oxidized carbon species when C₆₀ is deposited onto neutral and partially doped e-P3HT films. The changes in spectral intensity are summarized in Table SI3.1. The largest charge redistribution was expected to occur in the neutral e-P3HT film; however, the data again suggests that the PF₆⁻ anions retained in the partially doped film served to stabilize the additional oxidized thiophenes that result from the interface dipole formation.² The concentration of oxidized thiophene actually slightly decreases in the fully oxidized e-P3HT film after the deposition of C₆₀, suggesting that the interface dipole formed as a result of some electron transfer from C₆₀ to the polymer. It was not possible to spectroscopically resolve the presence of C₆₀⁻ in any of the e-P3HT/C₆₀ heterojunctions, perhaps because of its low abundance, the overlap of its C 1s signal with other C 1s spectral features, and/or the absence of C₆₀⁻ altogether.

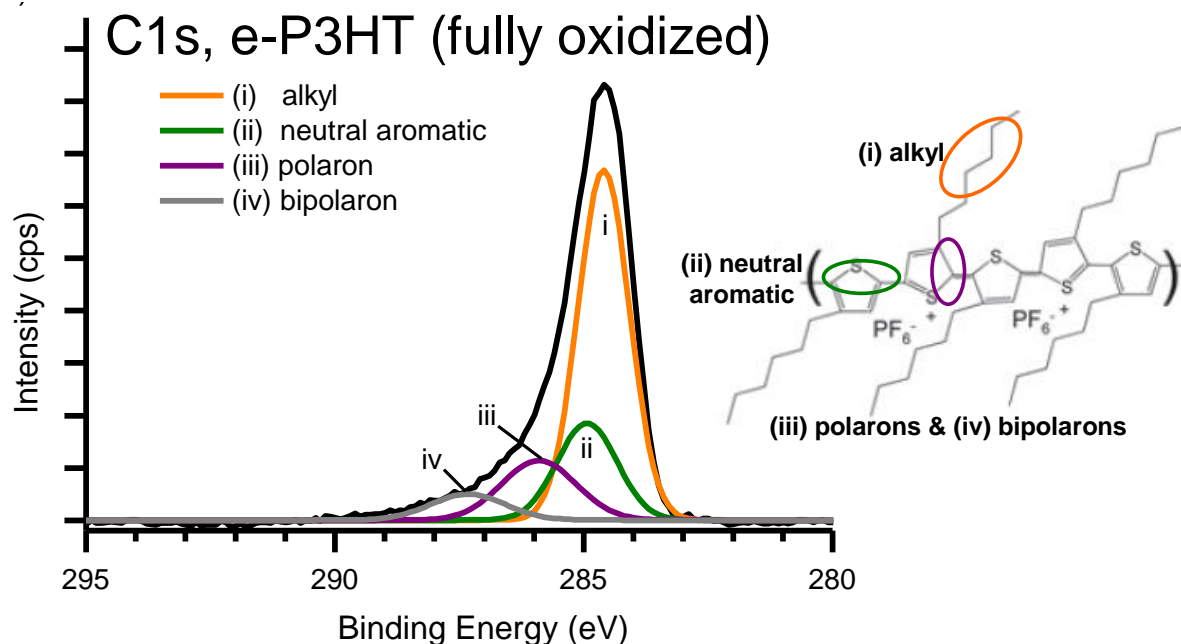


Figure SI3.1: The C 1s XPS spectrum of fully oxidized e-P3HT is comprised of four different carbon species. The alkyl carbons (i) yield photoelectrons with the lowest binding energy, and these carbons account for 60 % of the total C 1s spectral intensity regardless of the e-P3HT's doping level. The intensity from neutral aromatic carbons (ii) appears at a slightly higher binding energy. The magnitude of this peak changes with doping. When the film is neutral, this neutral aromatic signal contributes 40 % of the spectral intensity, but this signal decreases as the polymer is increasingly oxidized. The two higher binding energy features result from polaronic (iii) and bipolaronic (iv) carbons, and the intensities of these two signals also vary with doping.

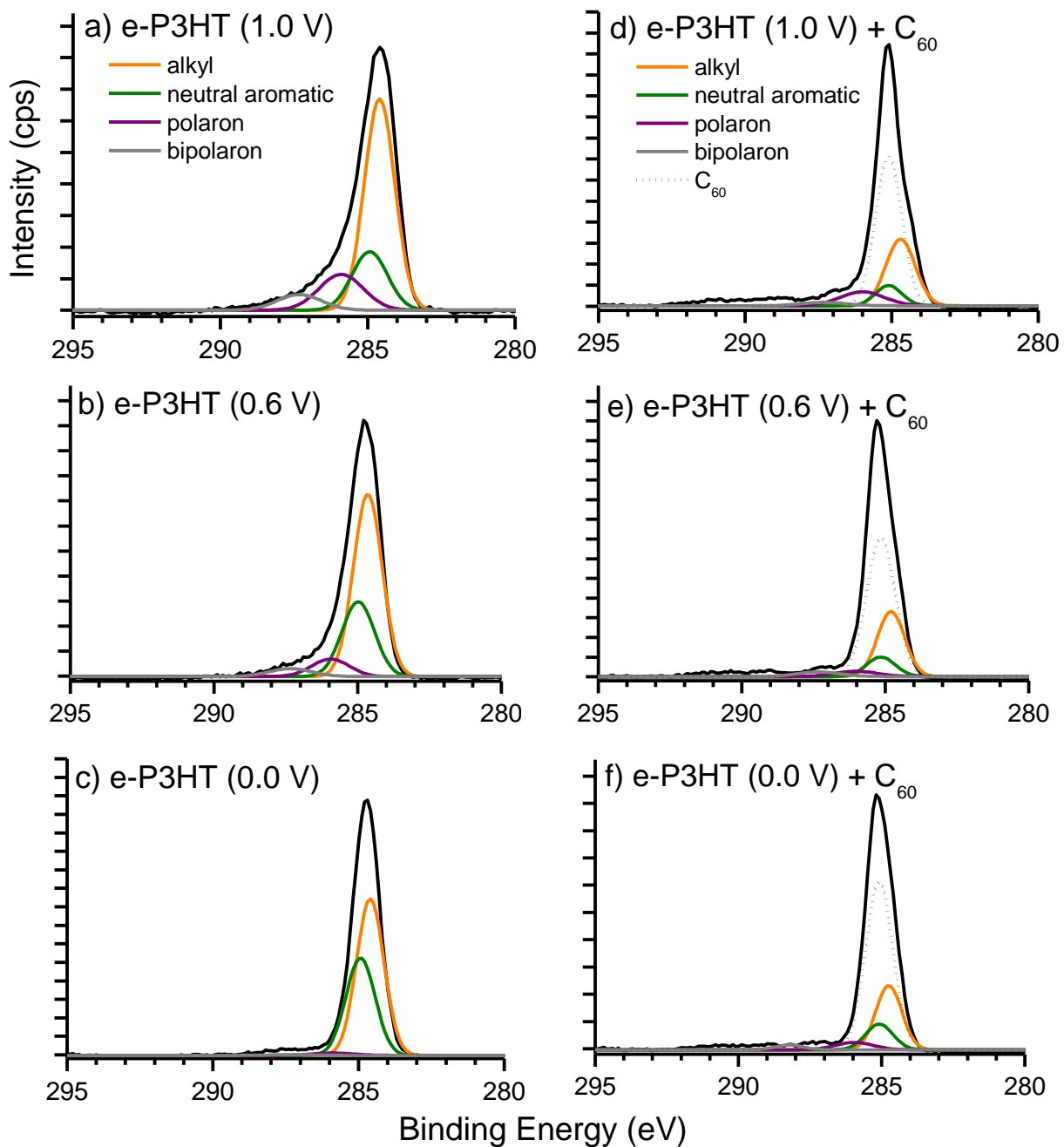


Figure SI3.2: The C 1s XPS spectra of the e-P3HT films before and after the deposition of C₆₀ illustrate the changing relative concentrations of neutral and oxidized e-P3HT on the highlydoped (a,d), partially doped (b, e), and undoped (c, f) polymer films. These changes were quantified with peak fitting as summarized in Table SI3.1.

Table SI3.1: Analysis of the e-P3HT C 1s XPS as a function of doping, increasing C₆₀ coverage

Highly doped e-P3HT (+ 1.0 V)

	0 nm C ₆₀	0.3 nm C ₆₀	0.6 nm C ₆₀	1.2 nm C ₆₀	2.4 nm C ₆₀
% alkyl	60	60	60	60	60
% neutral aromatic polymer	19	19	20	22	21
% polaron	15	15	16	14	13
% bipolaron	6	5	4	4	6
% e-P3HT C 1s Oxidized	21	20	20	18	19

Partially doped e-P3HT (+ 0.6 V)

	0 nm C ₆₀	0.3 nm C ₆₀	0.6 nm C ₆₀	1.2 nm C ₆₀	2.4 nm C ₆₀
% alkyl	60	60	60	60	60
% neutral aromatic polymer	28	25	22	19	19
% polaron	8	11	12	14	14
% bipolaron	4	4	6	7	7
% e-P3HT C 1s Oxidized	12	15	18	21	21

undoped e-P3HT (0.0 V)

	0 nm C ₆₀	0.3 nm C ₆₀	0.6 nm C ₆₀	1.2 nm C ₆₀	2.4 nm C ₆₀
% alkyl	59	60	60	60	60
% neutral aromatic polymer	39	33	31	28	25
% polaron	1.4	5	6	8	10
% bipolaron	0.4	2	3	4	5
% e-P3HT C 1s Oxidized	1.8	7	9	12	15

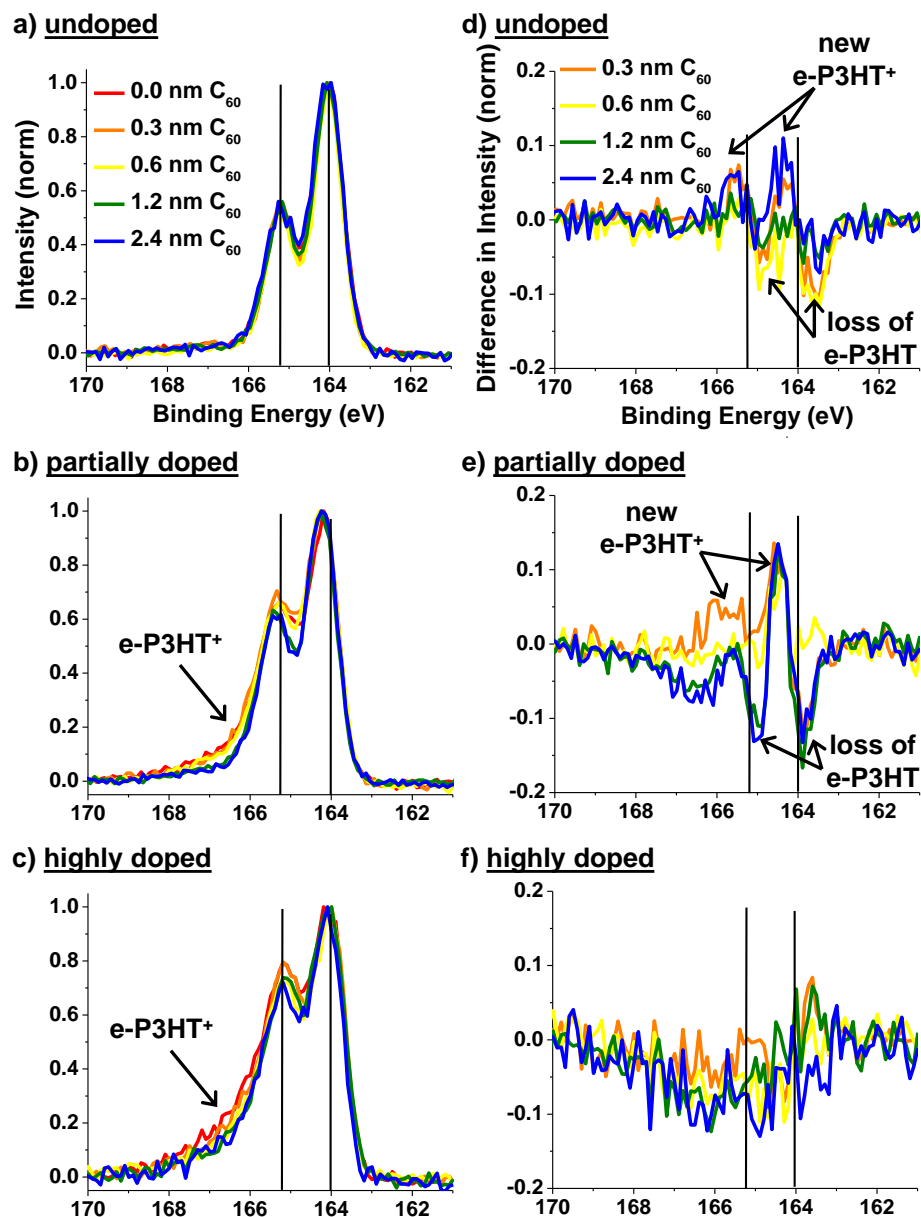


Figure SI3.3: The S 2p XPS spectra for the polymer films as C_{60} is deposited at the e-P3HT/ C_{60} interface include spectra for the undoped (a), partially doped (b) and highly doped (c) e-P3HT films. The red spectra are the polymer by itself, and the additional spectra are the polymer after increasing amounts of C_{60} are deposited onto the polymer film. The black lines correspond to the peak energies expected for the neutral sulfur doublet. Difference spectra, where the e-P3HT spectrum was subtracted from the e-P3HT/ C_{60} spectra, highlight the increase in polaronic density when C_{60} is deposited on the undoped (d) and partially doped (e) polymer. There are decreases in photoemission intensity coming from neutral sulfur, and increases in signal at higher binding energies, suggesting an increase in polaronic density as the e-P3HT came into contact with the C_{60} , consistent with partial electron transfer into the C_{60} . When the polymer is highly doped (f), there is slight de-doping of the e-P3HT film as indicated by the decrease in photoemission intensity and higher binding energies.

Table SI3.2: Analysis of the e-P3HT S 2p XPS as a function of doping, increasing C₆₀ coverage. Fluorine to sulfur peak intensity ratios (after correction by appropriate sensitivity factors) are added for reference.

Highly doped e-P3HT (+ 1.0 V)

	0 nm C₆₀	0.3 nm C₆₀	0.6 nm C₆₀	1.2 nm C₆₀	2.4 nm C₆₀
% neutral	54	54	57	60	59
% polaron	32	33	30	32	28
% bipolaron	14	13	13	8	13
% Oxidized	46	46	43	40	41
F 1s / S 2p	0.768	0.743	0.735	0.589	0.522

Partially doped e-P3HT (+ 0.6 V)

	0 nm C₆₀	0.3 nm C₆₀	0.6 nm C₆₀	1.2 nm C₆₀	2.4 nm C₆₀
% neutral	65	63	58	58	59
% polaron	25	28	33	31	33
% bipolaron	10	9	9	9	8
% Oxidized	35	37	42	42	41
F 1s / S 2p	0.455	0.444	0.328	0.269	0.269

undoped e-P3HT (0.0 V)

	0 nm C₆₀	0.3 nm C₆₀	0.6 nm C₆₀	1.2 nm C₆₀	2.4 nm C₆₀
% neutral	95	85	88	86	82
% polaron	4	11	10	11	13
% bipolaron	1	4	2	3	5
% Oxidized	5	15	12	14	18

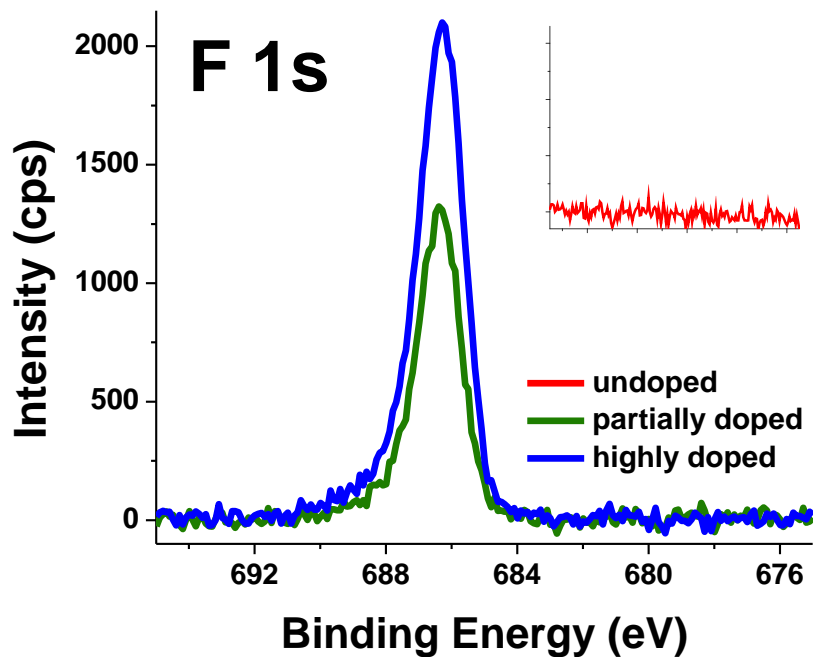


Figure SI3.4: Fluorine 1s XPS spectra indicate that the PF_6^- counter ion was retained in the partially doped and highly doped e-P3HT films. No evidence of PF_6^- is observed for the undoped e-P3HT film over the same binding energy range (inset).

SI4: Additional e-P3HT/C₆₀ UPS spectra

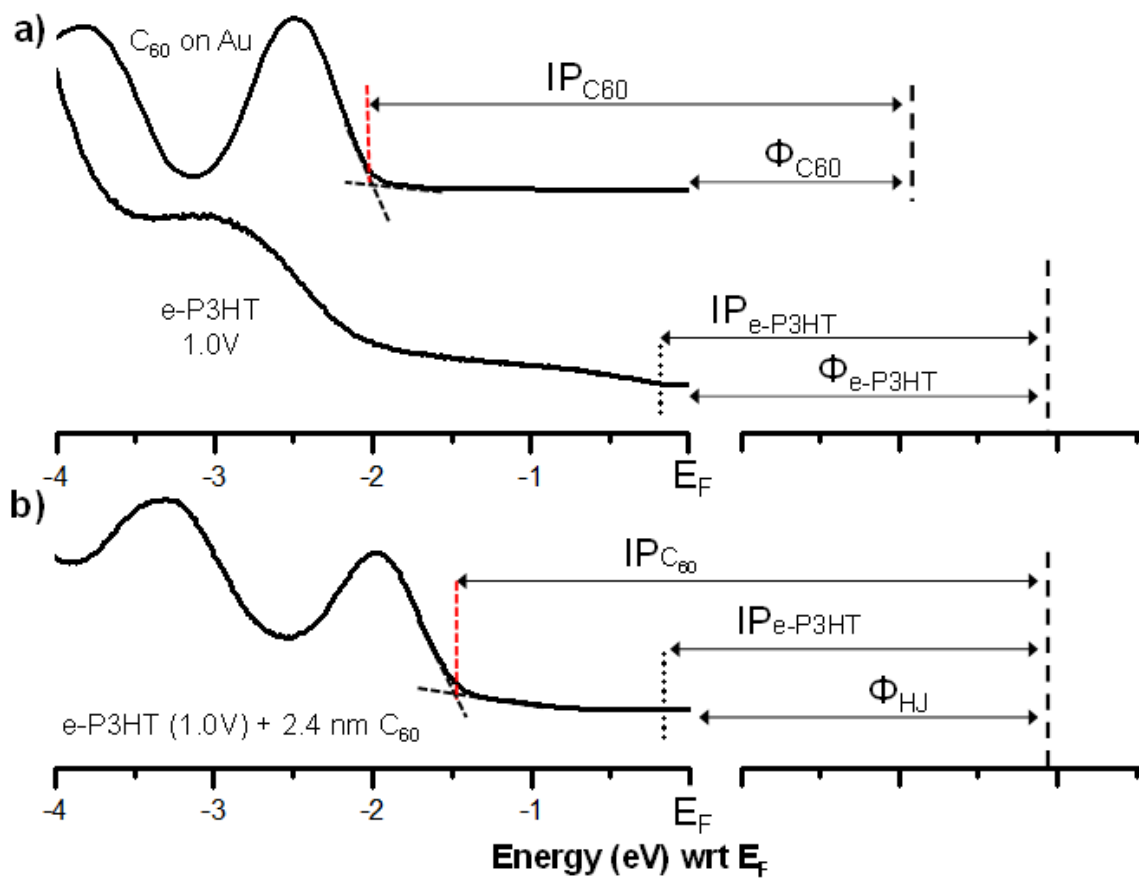


Figure SI4.1: UPS spectra were used to determine ionization potentials and work functions of e-P3HT and e-P3HT/C₆₀ heterojunctions. Bulk values for the polymer and fullerene were calculated from the spectra in (a), while the heterojunction values were calculated from spectra like the highly doped e-P3HT/C₆₀ spectrum in (b).

Table SI4.1: UPS analysis of the e-P3HT and e-P3HT/C₆₀ heterojunction valence electronic structure determined as described above. The e-P3HT work function ($\Phi_{\text{e-P3HT}}$) and ionization potential ($\text{IP}_{\text{e-P3HT}}$) were taken from the e-P3HT films before the deposition of any C₆₀. Values marked “HJ” were measured after 2.4 nm of C₆₀ had been deposited. The difference between the e-P3HT work function and the work function of the e-P3HT heterojunction is labeled $\Delta\Phi$.

Sample	$\Phi_{\text{e-P3HT}}$	$\text{IP}_{\text{e-P3HT}}$	Φ_{HJ}	$\text{IP}_{\text{e-P3HT}}$ (HJ)	IP_{C60} (HJ)	$\Delta\Phi$
Highly doped e-P3HT	5.0	5.1	4.9	5.1	6.3	-0.1 eV
Partially doped e-P3HT	4.8	4.9	4.5	4.7	6.3	-0.3 eV
Undoped e-P3HT	4.1	4.3	4.0	4.4	6.1	-0.1 eV

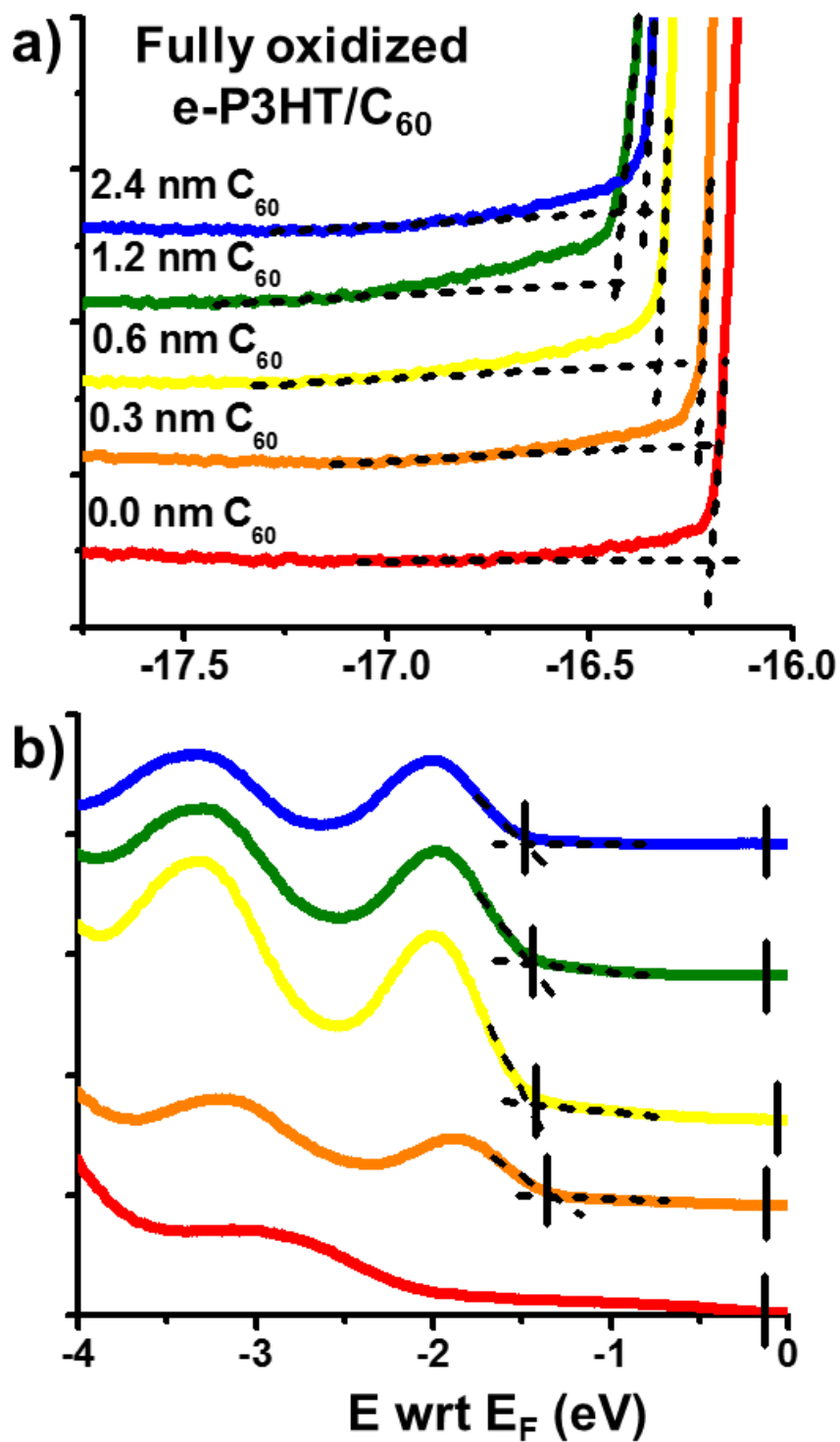


Figure SI4.2: The secondary edge (a) and the high kinetic energy edge (b) for the highly doped e-P3HT film (red) and the e-P3HT film plus increasing amounts of C₆₀ (orange – blue). Dashed lines illustrate how values for Φ , IP_{e-P3HT} , and IP_{C60} were determined.

Table SI4.2: Raw values for the features in Figure SI4.2. The standard deviations come from the average of three different spots on the same sample. The error of the instrument is ± 0.1 eV. The work function, IP_{e-P3HT} , and IPC_{60} in Table SI4.1 are calculated as the onset of the feature $- 21.2$ eV (the energy of the He(I) photon).

nm C₆₀	2° edge (wrt E_F)	onset e-P3HT (wrt E_F)	onset C₆₀ (wrt E_F)
0	-16.19 eV \pm 0.02 eV	-0.14 eV \pm 0.02 eV	
0.3	-16.20 eV \pm 0.02 eV	-0.14 eV \pm 0.06 eV	-1.26 eV \pm 0.02 eV
0.6	-16.30 eV \pm 0.02 eV	-0.08 eV \pm 0.01 eV	-1.43 eV \pm 0.03 eV
1.2	-16.30 eV \pm 0.02 eV	-0.14 eV \pm 0.15 eV	-1.39 eV \pm 0.03 eV
2.4	-16.30 eV \pm 0.02 eV	-0.16 eV \pm 0.03 eV	-1.47 eV \pm 0.01 eV

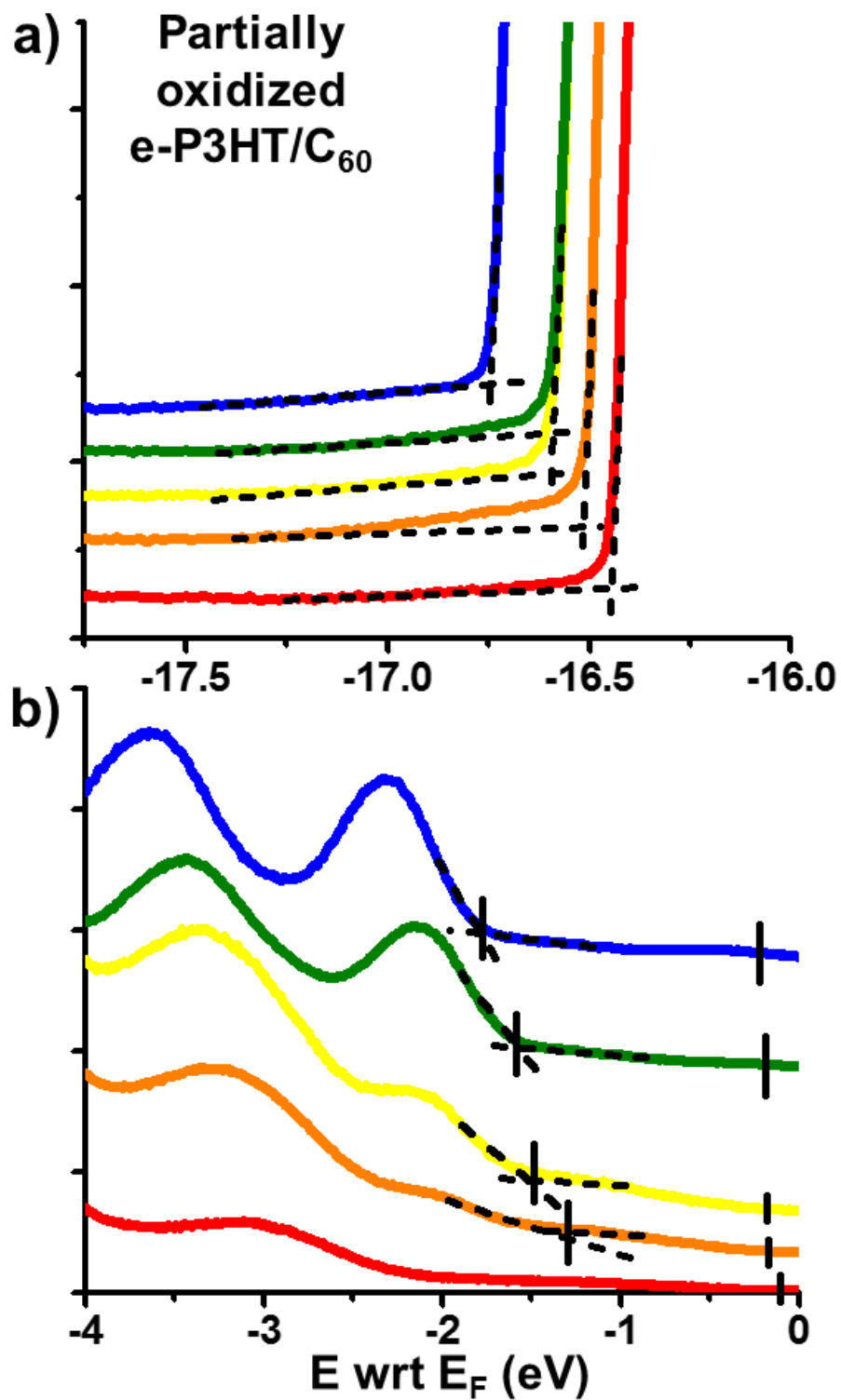


Figure SI4.3: The secondary edge (a) and the high kinetic energy edge (b) for the partially doped e-P3HT film (red) and the e-P3HT film plus increasing amounts of C₆₀ (orange – blue). Dashed lines illustrate how values for Φ , IP_{e-P3HT} , and IP_{C60} were determined.

Table SI4.3: Raw values for the features in Figure SI4.3. The standard deviations come from the average of three different spots on the same sample. The error of the instrument is ± 0.1 eV. The work function, IP_{e-P3HT} , and IPC_{60} in Table SI4.1 are calculated as the onset of the feature $- 21.2$ eV (the energy of the He(I) photon).

nm C₆₀	2° edge (wrt E_F)	onset e-P3HT (wrt E_F)	onset C₆₀ (wrt E_F)
0	-16.44 eV \pm 0.01 eV	-0.10 eV \pm 0.02 eV	
0.3	-16.50 eV \pm 0.01 eV	-0.19 eV \pm 0.04 eV	-1.09 eV \pm 0.05 eV
0.6	-16.54 eV \pm 0.01 eV	-0.17 eV \pm 0.03 eV	-1.30 eV \pm 0.01 eV
1.2	-16.52 eV \pm 0.04 eV	-0.15 eV \pm 0.04 eV	-1.51 eV \pm 0.04 eV
2.4	-16.69 eV \pm 0.03 eV	-0.20 eV \pm 0.08 eV	-1.74 eV \pm 0.03 eV

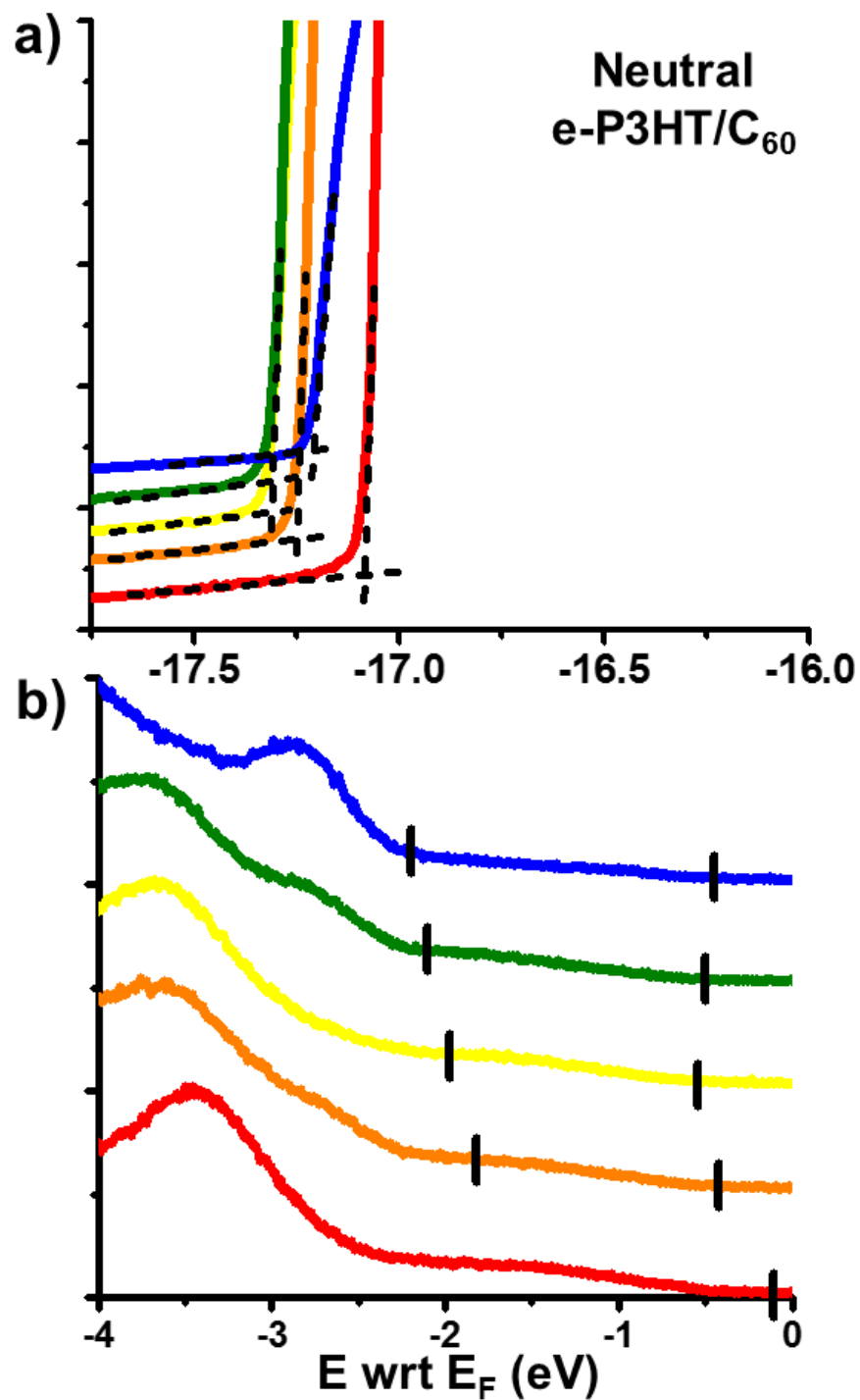


Figure SI4.4: The secondary edge (a) and the high kinetic energy edge (b) for the undoped e-P3HT film (red) and the e-P3HT film plus increasing amounts of C₆₀ (orange – blue). Dashed lines illustrate how values for Φ , IP_{e-P3HT} , and IP_{C60} were determined.

Table SI4.4: Raw values for the features in Figure SI4.4. The standard deviations come from the average of three different spots on the same sample. The error of the instrument is ± 0.1 eV. The work function, IP_{e-P3HT} , and IPC_{60} in Table SI4.1 are calculated as the onset of the feature $- 21.2$ eV (the energy of the He(I) photon).

nm C₆₀	2° edge (wrt E_F)	onset e-P3HT (wrt E_F)	onset C₆₀ (wrt E_F)
0	-17.07 eV \pm 0.01 eV	-0.21 eV \pm 0.01 eV	
0.3	-17.20 eV \pm 0.08 eV	-0.40 eV \pm 0.17 eV	-1.73 eV \pm 0.20 eV
0.6	-17.31 eV \pm 0.01 eV	-0.56 eV \pm 0.08 eV	-1.90 eV \pm 0.10 eV
1.2	-17.31 eV \pm 0.03 eV	-0.54 eV \pm 0.07 eV	-1.94 eV \pm 0.04 eV
2.4	-17.23 eV \pm 0.01 eV	-0.42 eV \pm 0.20 eV	-2.14 eV \pm 0.05 eV

References:

1. (a) Clarke, T. M.; Durrant, J. R. *Chem. Rev.* **2010**, *110* (11), 6736-6767; (b) Giebink, N. C.; Lassiter, B. E.; Wiederrecht, G. P.; Wasielewski, M. R.; Forrest, S. R. *Phys. Rev. B: Condens. Matter* **2010**, *82* (15); (c) Giebink, N. C.; Wiederrecht, G. P.; Wasielewski, M. R.; Forrest, S. R. *Phys. Rev. B: Condens. Matter* **2010**, *82* (15); (d) Potscavage, W. J., Jr.; Sharma, A.; Kippelen, B. *Acc. Chem. Res.* **2009**, *42* (11), 1758-1767; (e) Potscavage, W. J.; Yoo, S.; Kippelen, B. *Appl. Phys. Lett.* **2008**, *93* (19); (f) Shockley, W.; Queisser, H. J. *J. Appl. Phys.* **1961**, *32* (3), 510-&; (g) Vandewal, K.; Tvingstedt, K.; Gadisa, A.; Inganas, O.; Manca, J. V. *Phys. Rev. B: Condens. Matter* **2010**, *81* (12); (h) Veldman, D.; Meskers, S. C. J.; Janssen, R. A. J. *Adv. Funct. Mater.* **2009**, *19* (12), 1939-1948.
2. (a) Ratcliff, E. L.; Jenkins, J. L.; Nebesny, K.; Armstrong, N. R. *Chem. Mater.* **2008**, *20* (18), 5796-5806; (b) Ratcliff, E. L.; Lee, P. A.; Armstrong, N. R. *J. Mater. Chem.* **2010**, *20* (13), 2672-2679.
3. (a) Chen, T.; Howells, S.; Gallagher, M.; Yi, L.; Sarid, D.; Lichtenberger, D. L.; Nebesny, K. W.; Ray, C. D. *J. Vac. Sci. Technol., B* **1992**, *10* (1), 170-174; (b) Lichtenberger, D. L.; Jatcko, M. E.; Nebesny, K. W.; Ray, C. D.; Huffman, D. R.; Lamb, L. D. *Abstr. Pap. Am. Chem. S.* **1991**, *201*, 94-COLL; (c) Lichtenberger, D. L.; Nebesny, K. W.; Ray, C. D.; Huffman, D. R.; Lamb, L. D. *Chem. Phys. Lett.* **1991**, *176* (2), 203-208.